

Partially implicit Runge-Kutta methods for wave-like equations in spherical-type coordinates

I. Cordero-Carrión · P. Cerdá-Durán

Received: date / Accepted: date

Abstract Partially implicit Runge-Kutta methods are presented in this work in order to numerically evolve in time a set of partial differential equations. These methods are designed to overcome numerical instabilities appearing during the evolution of a system of equations due to potential numerical unstable terms in the sources, such as stiff terms or the presence of factors as a result of a particular chosen system of coordinates. In this article, partially implicit Runge-Kutta methods for several convergence orders have been derived and stability properties have been analyzed. These methods are shown to be appropriated to avoid the development of numerical instabilities in the evolution in time of wave-like equations in spherical-type coordinates, in contrast to the explicit Runge-Kutta methods.

Keywords partial differential equations · numerical instabilities · wave equation · spherical coordinates

Mathematics Subject Classification (2010) 35L60 · 35L05 · 83C35

1 Introduction

The evolution in time of many complex systems, governed by partial differential equations (PDE), implies, in a broad variety of cases, looking for the numerical solution of a system of ordinary differential equations (ODEs). The most commonly used methods to integrate in time these systems of ODEs are the well-known Runge-Kutta (RK) ones (see e.g. [1] for a general review of these methods and their main properties). Several classifications of the RK methods can be done, according to, e.g., their convergence order, the number of stages or their explicit/implicit structure.

I. Cordero-Carrión
Max-Planck Institute for Astrophysics, Karl-Schwarschild-Str. 1, D-85741 Garching, Germany
E-mail: chabela@mpa-garching.mpg.de

P. Cerdá-Durán
Departamento de Astronomía y Astrofísica, University of Valencia, C/ Dr. Moliner, 50, E-46100 Burjassot, Spain
E-mail: pablo.cerda@uv.es

Implicit or partially implicit methods are used to deal with systems which require a special numerical treatment in order to have a stable evolution. The origin of the numerical instabilities in the evolution of a system of equations is diverse. Stiff terms in the sources of the equations can lead to the development of numerical instabilities when explicit RK (ERK) methods are used. In this context, the so-called implicit-explicit (IMEX) RK methods have been used to evolve in time conservation laws with stiff terms or convection-diffusion-reaction equations [2, 3, 4, 5].

Not only stiff terms can be the reason of the appearance of numerical instabilities. Source terms of the equations, when a particular system of coordinates is chosen, may introduce factors which can also be numerically interpreted as stiff terms. This fact will be evident for a wave equation in spherical coordinates in the numerical examples shown in Sect. 4, in which the $1/r^p$ factors, $p \in \mathbb{N}$, appearing due to spherical coordinates are interpreted as stiff terms close to $r = 0$, even when the evolved data is regular. In the case of the development of these numerical instabilities, an implicit treatment of the system offers a solution to get a stable evolution.

The implicit treatment of the sources needs, in general, an inversion of some operators. Depending on the complexity of the equations, the inversion can be done analytically or numerically, or be even prohibitive in practice from the numerical point of view. We will focus on a particular structure of equations which does not require any analytical or numerical inversion. Therefore, these methods have a computational cost similar to the ERK methods but they are able to provide stable evolutions due to their partially implicit component.

The choice of the coefficients in the derivation of the methods presented in this work are based on stability properties for both explicit and implicit parts, as it is described in the following sections. The stable evolution obtained for a particular example shows their validity. However, potential applications in other systems of equations have still to be checked.

The manuscript is organized as follows. In Sect. 2 the structure of the system of equations and the requirements for the numerical scheme are described. In Sect. 3, partially implicit RK (PIRK) methods, from first to third order, are derived; some comments concerning the derived PIRK methods and some available IMEX ones are mentioned. Numerical experiments are shown in Sect. 4, where PIRK methods are used to evolve in time a wave equation in spherical coordinates. Conclusions are drawn in Sect. 5.

2 Structure of the equations and requirements for the numerical methods

Let us consider the following system of PDEs,

$$\begin{cases} u_t = \mathcal{L}_1(u, v), \\ v_t = \mathcal{L}_2(u) + \mathcal{L}_3(u, v), \end{cases} \quad (1)$$

being \mathcal{L}_1 , \mathcal{L}_2 and \mathcal{L}_3 general non-linear differential operators. Let us denote by L_1 , L_2 and L_3 their discrete operators, respectively. No restrictions onto the discrete operators are imposed. They can correspond, for example, to a flux-conservative numerical scheme of a conservation law or a finite difference scheme of a general evolution system.

L_1 and L_3 will be treated into an explicit way, whereas the L_2 operator will be considered to contain the unstable terms and, therefore, treated partially implicitly. Each stage of the RK method will proceed into two steps: i) the variable u is evolved explicitly; ii) the variable v is evolved taking into account the updated value of u for the evaluation of the L_2 operator. This strategy implies that the computational costs of the methods are comparable to those of the explicit ones. The resulting numerical schemes do not need any analytical or numerical inversion, in the same way as ERK methods do not, but the partially implicit treatment confers stability to the numerical algorithm.

Numerical methods based on a nonlinear stability requirement are very desirable. Such methods were originally named as total variation diminishing (TVD) and are also referred to as strong stability preserving (SSP) methods (see e.g. [6, 7]). If $U = U(t)$ is a vector of discretized variables, i.e., $[U(t)]_j = U_j(t) = u(x_j, t)$, and u_j^n is the numerical approximation to $u(x_j, t_n)$, then SSP discretizations have the property that the total variation

$$TV(U^n) = \sum_j |u_j^n - u_{j-1}^n| \quad (2)$$

of the numerical solution does not increase with time, i.e.,

$$TV(U^{n+1}) \leq TV(U^n). \quad (3)$$

A sequence U^n is said to be strongly stable in a given norm $\|\cdot\|$ provided that $\|U^{n+1}\| \leq \|U^n\|$ for all $n > 0$. The choice of the norm is arbitrary, being the TV-norm, and the infinity norm, two natural possibilities.

A s -stage ERK method for the equation $\partial_t U = L(U)$ can be written in the form:

$$\begin{aligned} U^{(0)} &= U^n, \\ U^{(i)} &= \sum_{k=0}^{i-1} \left(\alpha_{ik} U^{(k)} + \Delta t \beta_{ik} L(U^{(k)}) \right), \\ &\quad i = 1, 2, \dots, s, \\ U^{n+1} &= U^{(s)}, \end{aligned} \quad (4)$$

where all the $\alpha_{ik} \geq 0$, and $\alpha_{ik} = 0$ only if $\beta_{ik} = 0$, and Δt denotes the time step. Gottlieb and Shu [6] proved that the classical second-order method,

$$\begin{aligned} U^{(0)} &= U^n, \\ U^{(1)} &= U^n + \Delta t L(U^n), \\ U^{n+1} &= \frac{1}{2} U^n + \frac{1}{2} U^{(1)} + \frac{1}{2} \Delta t L(U^{(1)}), \end{aligned} \quad (5)$$

is the optimal second-order two-stage SSP ERK method, and that the third-order one due to Shu and Osher [8],

$$\begin{aligned} U^{(0)} &= U^n, \\ U^{(1)} &= U^n + \Delta t L(U^n), \\ U^{(2)} &= \frac{3}{4} U^n + \frac{1}{4} U^{(1)} + \frac{1}{4} \Delta t L(U^{(1)}), \\ U^{n+1} &= \frac{1}{3} U^n + \frac{2}{3} U^{(2)} + \frac{2}{3} \Delta t L(U^{(2)}), \end{aligned} \quad (6)$$

is the optimal third-order three-stage SSP ERK method. The optimal adjective refers, for a given number of stages, to a maximization of the corresponding Courant-Friedrichs-Lewy (CFL) value (1 in both cases) and the efficiency in the storage requirement.

This property is crucial to capture the right behavior of the evolution of the system. In the derivation of the PIRK methods proposed in this work, the previously described optimal SSP RK methods are recovered when the L_2 operator is neglected, i.e., when partially implicitly treated parts are not taken into account.

Positiveness of the coefficients is preferable. See [1, 9] for more details about the implications of positive/negative coefficients on stability properties and storage requirements. The PIRK methods derived minimize the number of stages, two and three in the case of second and third-order methods, respectively. They differ, among other aspects, from the explicit, singly diagonally implicit RK ones [10] by not having an explicit first stage. Taking into account previous considerations, the remaining coefficients associated to the L_2 operator for the different methods are chosen according to stability criteria.

The requirements for the numerical algorithm to solve the system (1) are summarized in the following points:

- i) RK method, with at most a singly diagonally implicit RK scheme for the implicit part.
- ii) Positive coefficients are preferable.
- iii) Recovery of the optimal SSP ERK methods when implicitly treated parts are neglected.
- iv) Choice of the remaining coefficients according to stability criteria.

3 Numerical methods and stability analysis

In this section, the PIRK methods, from first to third order, are derived. The methods for a particular convergence order and equal number of stages, and imposing SSP optimal ERK methods for the pure explicitly treated parts are deduced; next, stability analysis is carried out and optimal values for the remaining coefficients are selected, with preference to positive coefficients.

3.1 Stability definitions

Numerical methods combining explicit and implicit treatments can be analyzed in several ways from the stability point of view. Let us consider the scalar complex test equation,

$$\partial_t y(t) = \bar{\nu} y(t) + \bar{\mu} y(t), \quad (7)$$

where $y(t)$ is the evolved variable, and $\bar{\nu}$ and $\bar{\mu}$ denote the eigenvalues corresponding to the explicit and implicit operators, respectively. Let us define $\nu := \bar{\nu} \Delta t$ and $\mu := \bar{\mu} \Delta t$, where Δt is the time step of the RK method. When a particular RK scheme is applied to Eq. (7), the updated value of the evolved variable, y^{n+1} , can be written in terms of its previous value, y^n , as

$$y^{n+1} = R(\mu, \nu) y^n, \quad (8)$$

where $R(\mu, \nu)$ is a fraction of polynomials depending on μ and ν , called stability function. Stability thus requires that $|R(\mu, \nu)| \leq 1$.

Let us define

$$\mathcal{D}_0 := \left\{ \mu \in \mathbb{C} : \text{the scheme is stable for any } \nu \in \mathbb{C}^- \right\}. \quad (9)$$

Here, stability with respect to the implicit part is considered, and it has to be compared whether \mathcal{D}_0 is smaller than the stability region of the explicit method. Alternatively, one can insist on using the full stability region of the explicit method, and, in that case, the following set has to be taken into account:

$$\mathcal{D}_1 := \left\{ \nu \in \mathbb{C} : \text{the scheme is stable for any } \mu \in \mathbb{C}^-, |1 + \mu| \leq 1 \right\}. \quad (10)$$

In this article we will focus on the set \mathcal{D}_1 from now on. A SSP ERK method is recovered when implicitly treated parts are neglected. This property guarantees the stability of the pure explicit parts. The stability analysis will concern the addition of the partially implicit component.

Since we are considering a system of equations, and the characteristic structure of eigenvalues and eigenvectors of the explicit and implicit parts do not coincide necessarily, the previous analysis has to involve matrices instead of scalars, and the global structure of the system has to be taken into account. Let us denote $(\bar{\alpha}_1 u, \bar{\alpha}_2 v)$, $\bar{\lambda} u$ and $(\bar{\gamma}_1 u, \bar{\gamma}_2 v)$ the associated linearized parts of the \mathcal{L}_1 , \mathcal{L}_2 and \mathcal{L}_3 operators, respectively. The linearized system (1) is then rewritten as

$$\begin{cases} u_t = \bar{\alpha}_1 u + \bar{\alpha}_2 v, \\ v_t = \bar{\gamma}_1 u + \bar{\gamma}_2 v + \bar{\lambda} u. \end{cases} \quad (11)$$

Let us denote $\alpha_i := \bar{\alpha}_i \Delta t$, $\lambda := \bar{\lambda} \Delta t$ and $\gamma_i := \bar{\gamma}_i \Delta t$. A stability function and its absolute value will be replaced by a stability matrix and the absolute values of its eigenvalues. The hypothesis $|1 + \mu| \leq 1$ will be replaced by $|\omega_i| \leq 1$, where ω_i , $i = 1, 2$ denote the two eigenvalues of the matrix regarding the explicit part

$$\begin{pmatrix} 1 + \alpha_1 & \alpha_2 \\ \gamma_1 & 1 + \gamma_2 \end{pmatrix}. \quad (12)$$

This condition implies, in particular, that the determinant of previous matrix, denoted by dex , and its trace, denoted by trex , are bounded as follows:

$$|\text{dex}| = |\omega_1| |\omega_2| = |(1 + \alpha_1)(1 + \gamma_2) - \alpha_2 \gamma_1| \leq 1, \quad (13)$$

$$|\text{trex}| = |\omega_1 + \omega_2| = |2 + \alpha_1 + \gamma_2| \leq 2. \quad (14)$$

Moreover, in the condition $|R(\mu, \nu)| \leq 1$, the stability function $R(\mu, \nu)$ will be replaced by the two eigenvalues associated to the matrix M , M defined such that

$$\begin{pmatrix} u^{n+1} \\ v^{n+1} \end{pmatrix} = M \begin{pmatrix} u^n \\ v^n \end{pmatrix}, \quad (15)$$

for a given method. However, in order to simplify the derivation of the PIRK methods, we are going to relax the bound on the eigenvalues of M by a bound on its determinant, i.e., $|\det(M)| \leq 1$. The restriction onto the eigenvalues will be recovered in the numerical experiments in Sect. 4 as the boundaries of the stability region.

We also assume that $\text{Re}(\lambda \alpha_2) \leq 0$, where Re denotes the real part of a complex number. This condition is satisfied for general sinusoidal wave-like equations written as a first-order system in time (see Sect. 4 for examples).

3.2 First-order method

The derived one-stage first-order method for the system (1) can be written in terms of one coefficient, c_1 , as follows:

$$\begin{cases} u^{n+1} = u^n + \Delta t L_1(u^n, v^n), \\ v^{n+1} = v^n + \Delta t \left[(1 - c_1)L_2(u^n) + c_1L_2(u^{n+1}) + L_3(u^n, v^n) \right]. \end{cases} \quad (16)$$

A Taylor expansion of (u^{n+1}, v^{n+1}) and all the operators in terms of (u^n, v^n) and their spatial derivatives was carried out to guarantee the convergence order of the method. This method is a particular case for the system (1) of the so-called IMEX- θ method (see, e.g., [11]), where c_1 is the θ parameter.

System (16) can be written as

$$\begin{pmatrix} u^{n+1} \\ v^{n+1} \end{pmatrix} = M_1 \begin{pmatrix} u^n \\ v^n \end{pmatrix}, \quad (17)$$

where

$$M_1 = \begin{pmatrix} 1 + \alpha_1 & \alpha_2 \\ \gamma_1 + \lambda(1 + \alpha_1 c_1) & 1 + \gamma_2 + \lambda \alpha_2 c_1 \end{pmatrix}. \quad (18)$$

Its determinant is:

$$\det(M_1) = \text{dex} - \lambda \alpha_2 (1 - c_1). \quad (19)$$

Taking into account bound (13), $c_1 = 1$ guarantees $|\det(M_1)| \leq 1$, for all possible values of $\lambda \alpha_2$. The resulting method is:

$$\begin{cases} u^{n+1} = u^n + \Delta t L_1(u^n, v^n), \\ v^{n+1} = v^n + \Delta t \left[L_2(u^{n+1}) + L_3(u^n, v^n) \right]. \end{cases} \quad (20)$$

3.3 Second-order method

The derived two-stages second-order method for the system (1), imposing SSP optimal two-stages second-order method for the pure explicit parts (L_1 and L_3 operators), can be written in terms of two coefficients, (c_1, c_2) (do not confuse coefficient c_1 with the one appearing in the first-order method), as follows:

$$\begin{cases} u^{(1)} = u^n + \Delta t L_1(u^n, v^n), \\ v^{(1)} = v^n + \Delta t \left[(1 - c_1)L_2(u^n) + c_1L_2(u^{(1)}) + L_3(u^n, v^n) \right], \end{cases} \quad (21)$$

$$\begin{cases} u^{n+1} = \frac{1}{2} \left[u^n + u^{(1)} + \Delta t L_1(u^{(1)}, v^{(1)}) \right], \\ v^{n+1} = v^n + \frac{\Delta t}{2} \left[L_2(u^n) + 2c_2L_2(u^{(1)}) + (1 - 2c_2)L_2(u^{n+1}) \right. \\ \left. + L_3(u^n, v^n) + L_3(u^{(1)}, v^{(1)}) \right]. \end{cases} \quad (22)$$

A Taylor expansion of $(u^{(1)}, v^{(1)})$, (u^{n+1}, v^{n+1}) and all the operators in terms of (u^n, v^n) and their spatial derivatives was carried out to guarantee the convergence order of the method.

From (21) and (22),

$$\begin{pmatrix} u^{n+1} \\ v^{n+1} \end{pmatrix} = M_2 \begin{pmatrix} u^n \\ v^n \end{pmatrix}, \quad (23)$$

where

$$M_2 = \begin{pmatrix} 1 & 0 \\ (1/2 - c_2)\lambda & 1 \end{pmatrix} \left[\begin{pmatrix} 1/2 & 0 \\ (\lambda + \gamma_1)/2 & 1 + \gamma_2/2 \end{pmatrix} + \frac{1}{2} \begin{pmatrix} 1 + \alpha_1 & \alpha_2 \\ \gamma_1 + 2\lambda c_2 & \gamma_2 \end{pmatrix} \begin{pmatrix} 1 + \alpha_1 & \alpha_2 \\ \gamma_1 + \lambda(1 + \alpha_1 c_1) & 1 + \gamma_2 + \lambda\alpha_2 c_1 \end{pmatrix} \right]. \quad (24)$$

Its determinant is:

$$\det(M_2) = \frac{1}{4} \left[(1 - \text{dex})^2 + \text{trex}^2 + \lambda\alpha_2(1 - \text{dex})(1 - 2c_1 + 2c_2) + \lambda^2\alpha_2^2(2c_2 - c_1 - 2c_1c_2) \right]. \quad (25)$$

The conditions $1 - 2c_1 + 2c_2 = 2c_2 - c_1 - 2c_1c_2 = 0$ guarantee $|\det(M_2)| \leq 1$, for all possible values of $\lambda\alpha_2$. But they lead to $c_1 = (1 \pm i)/2 \notin \mathbb{R}$, $c_2 = \pm i/2 \notin \mathbb{R}$, where $i = \sqrt{-1}$ is the imaginary unit.

Let us restrict to real numbers, so $\omega_i \in \mathbb{R}$ and $\lambda\alpha_2 \in \mathbb{R}^-$. $|\det(M_2)| \leq 1$ is then equivalent to:

$$-4 \leq K_1 + \lambda\alpha_2 K_2(1 - 2c_1 + 2c_2) + \lambda^2\alpha_2^2(2c_2 - c_1 - 2c_1c_2) \leq 4, \quad (26)$$

where

$$K_1 := (1 - \text{dex})^2 + \text{trex}^2 = 1 + \omega_1^2\omega_2^2 + \omega_1^2 + \omega_2^2 \in [1, 4] \quad (27)$$

and

$$K_2 := 1 - \text{dex} \in [0, 2]. \quad (28)$$

The minimum value of K_1 is reached for $\omega_1 = \omega_2 = 0$. The maximum value of K_1 is reached for $\omega_1^2 = \omega_2^2 = 1$. The minimum value of K_2 is reached for $\omega_1 = \omega_2 = \pm 1$. The maximum value of K_2 is reached for $\omega_1 = -\omega_2 = \pm 1$. For $\omega_1 = \omega_2 = 0$, $K_2 = 1$.

We analyze the value of $\det(M_2)$ for $\omega_i = 0, \pm 1$, $i = 1, 2$, and in the cases $|\lambda\alpha_2| \gg 1$, $\lambda\alpha_2 \approx -1$ and $|\lambda\alpha_2| \ll 1$. The resulting sufficient conditions are (see Appendix A for more details):

$$\begin{aligned} 0 &\leq 2c_2(1 - c_1) - c_1, \quad 1 - 2c_1 + 2c_2 \leq 0, \\ 0 &\leq 6 + 5c_1 - 6c_2 + 2c_1c_2, \quad 0 \leq 4 + c_1 - 2c_1c_2, \end{aligned} \quad (29)$$

together with

$$-4 \leq \lambda\alpha_2(1 - 2c_1 + 2c_2), \quad -5 \leq \lambda^2\alpha_2^2(2c_2 - c_1 - 2c_1c_2). \quad (30)$$

For $|\lambda\alpha_2| \ll 1$, first inequality in (30) is the most relevant one of both. We impose $1 - 2c_1 + 2c_2 = 0$, and minimize $|2c_2(1 - c_1) - c_1|$ (taking into account (29)). The resulting values are $c_1 = 1/2$ and $c_2 = 0$. The scheme is then written as:

$$\begin{cases} u^{(1)} = u^n + \Delta t L_1(u^n, v^n), \\ v^{(1)} = v^n + \Delta t \left[\frac{1}{2} L_2(u^n) + \frac{1}{2} L_2(u^{(1)}) + L_3(u^n, v^n) \right], \end{cases} \quad (31)$$

$$\begin{cases} u^{n+1} = \frac{1}{2} \left[u^n + u^{(1)} + \Delta t L_1(u^{(1)}, v^{(1)}) \right], \\ v^{n+1} = v^n + \frac{\Delta t}{2} \left[L_2(u^n) + L_2(u^{n+1}) + L_3(u^n, v^n) + L_3(u^{(1)}, v^{(1)}) \right]. \end{cases} \quad (32)$$

For $|\lambda\alpha_2| \gg 1$, second inequality in (30) is the most relevant one of both. We impose $2c_2 - c_1 - 2c_1c_2 = 0$, and minimize $|1 - 2c_1 + 2c_2|$ (taking into account (29)). The resulting values are $c_1 = 1 - \sqrt{2}/2$ and $c_2 = (\sqrt{2} - 1)/2$. The scheme is written in this case as:

$$\begin{cases} u^{(1)} = u^n + \Delta t L_1(u^n, v^n), \\ v^{(1)} = v^n + \Delta t \left[\frac{\sqrt{2}}{2} L_2(u^n) + \left(1 - \frac{\sqrt{2}}{2}\right) L_2(u^{(1)}) + L_3(u^n, v^n) \right], \end{cases} \quad (33)$$

$$\begin{cases} u^{n+1} = \frac{1}{2} \left[u^n + u^{(1)} + \Delta t L_1(u^{(1)}, v^{(1)}) \right], \\ v^{n+1} = v^n + \frac{\Delta t}{2} \left[L_2(u^n) + (\sqrt{2} - 1)L_2(u^{(1)}) + (2 - \sqrt{2})L_2(u^{n+1}) \right. \\ \left. + L_3(u^n, v^n) + L_3(u^{(1)}, v^{(1)}) \right]. \end{cases} \quad (34)$$

Depending of the value of $|\lambda\alpha_2| = |\bar{\lambda}\bar{\alpha}_2|\Delta t^2$, it will be more convenient to use a particular set of values for the coefficients. For not too stiff numerical problems, the choice $(c_1, c_2) = (1/2, 0)$ will be more appropriated and it avoids to compute $L_2(u^{(1)})$ to obtain v^{n+1} in the final stage. For very stiff numerical problems, last option is better. This fact will be illustrated in Sect. 4.

3.4 Third-order method

The derived three-stages third-order method for the system (1), imposing SSP optimal three-stages third-order method for the pure explicit parts (L_1 and L_3 operators), can be written in terms of two coefficients, (c_1, c_2) (do not confuse these coefficients with the ones appearing in previous methods), as follows:

$$\begin{cases} u^{(1)} = u^n + \Delta t L_1(u^n, v^n), \\ v^{(1)} = v^n + \Delta t \left[(1 - c_1)L_2(u^n) + c_1 L_2(u^{(1)}) + L_3(u^n, v^n) \right], \end{cases} \quad (35)$$

$$\begin{cases} u^{(2)} = \frac{1}{4} \left[3u^n + u^{(1)} + \Delta t L_1(u^{(1)}, v^{(1)}) \right], \\ v^{(2)} = v^n + \frac{\Delta t}{4} \left[2(c_1 + 2c_2)L_2(u^n) + 4c_2 L_2(u^{(1)}) + 2(1 - c_1 - 4c_2)L_2(u^{(2)}) \right. \\ \left. + L_3(u^n, v^n) + L_3(u^{(1)}, v^{(1)}) \right], \end{cases} \quad (36)$$

$$\begin{cases} u^{n+1} = \frac{1}{3} \left[u^n + 2u^{(2)} + 2\Delta t L_1(u^{(2)}, v^{(2)}) \right], \\ v^{n+1} = v^n + \frac{\Delta t}{6} \left[L_2(u^n) + L_2(u^{(1)}) + 4L_2(u^{(2)}) \right. \\ \left. + L_3(u^n, v^n) + L_3(u^{(1)}, v^{(1)}) + 4L_3(u^{(2)}, v^{(2)}) \right], \end{cases} \quad (37)$$

A Taylor expansion of the values of the variables u and v in all the stages of the method and all the operators in terms of (u^n, v^n) and their spatial derivatives was carried out to guarantee the convergence order of the method.

From (35)-(37),

$$\begin{pmatrix} u^{n+1} \\ v^{n+1} \end{pmatrix} = M_3 \begin{pmatrix} u^n \\ v^n \end{pmatrix}, \quad (38)$$

where

$$M_3 = \begin{pmatrix} 1 + \frac{\alpha_1}{6} & \frac{\alpha_2}{6} \\ \frac{\gamma_1 + \lambda}{6} & 1 + \frac{\gamma_2}{6} \end{pmatrix} + \frac{1}{6} \begin{pmatrix} \alpha_1 & \alpha_2 \\ \gamma_1 + \lambda & \gamma_2 \end{pmatrix} N_1 \\ + \frac{2}{3} \begin{pmatrix} \alpha_1 & \alpha_2 \\ \gamma_1 + \lambda & \gamma_2 \end{pmatrix} N_2, \quad (39)$$

$$N_1 = \begin{pmatrix} 1 & 0 \\ \lambda c_1 & 1 \end{pmatrix} \begin{pmatrix} 1 + \alpha_1 & \alpha_2 \\ \gamma_1 + \lambda(1 - c_1) & 1 + \gamma_2 \end{pmatrix}, \quad (40)$$

$$N_2 = \begin{pmatrix} 1 & 0 \\ (1 - c_1 - 4c_2)\frac{\lambda}{2} & 1 \end{pmatrix} \left[\begin{pmatrix} 1 + \frac{\alpha_1}{4} & \frac{\alpha_2}{4} \\ \frac{\gamma_1}{4} + (c_1 + 2c_2)\frac{\lambda}{2} & 1 + \frac{\gamma_2}{4} \end{pmatrix} \right. \\ \left. + \begin{pmatrix} \frac{\alpha_1}{4} & \frac{\alpha_2}{4} \\ \frac{\gamma_1}{4} + \lambda c_2 & \frac{\gamma_2}{4} \end{pmatrix} N_1 \right]. \quad (41)$$

Its determinant is:

$$\det(M_3) = \frac{1}{36} \left[14 + 2(\text{trex} - 1)^3 + (\text{dex} - 2)^3 + 6\text{trex}^2 + 3\text{dex}((\text{trex} - 1)^2 - 2) \right] \\ + \frac{1}{24} \lambda \alpha_2 (-1 + c_1 - 4c_2) \left[(\text{dex} - 2)^2 + (\text{trex} - 1)^2 - 2 \right] \\ + \frac{1}{12} \lambda^2 \alpha_2^2 \left[c_1 - 4c_2 + (\text{dex} - 1)(4c_2 - c_1^2 - 4c_1 c_2) \right] \\ - \frac{1}{72} \lambda^3 \alpha_2^3 [-1 + 3(1 - 2c_1)(c_1 + 4c_2)]. \quad (42)$$

The expressions $-1 + c_1 - 4c_2$, $c_1 - 4c_2$, $4c_2 - c_1^2 - 4c_1 c_2$ and $-1 + 3(1 - 2c_1)(c_1 + 4c_2)$ cannot vanish simultaneously. Let us restrict, as in previous subsection, to real numbers, so $\omega_i \in \mathbb{R}$ and $\lambda \alpha_2 \in \mathbb{R}^-$. $|\det(M_3)| \leq 1$ is equivalent to:

$$-1 \leq \frac{K_3}{36} + \frac{\lambda \alpha_2 K_4 (-1 + c_1 - 4c_2)}{24} \\ + \frac{\lambda^2 \alpha_2^2}{12} [c_1 - 4c_2 + (\text{dex} - 1)(4c_2 - c_1^2 - 4c_1 c_2)] \\ - \frac{\lambda^3 \alpha_2^3}{72} [-1 + 3(1 - 2c_1)(c_1 + 4c_2)] \leq 1, \quad (43)$$

where

$$K_3 := 14 + 2(\text{trex} - 1)^3 + (\text{dex} - 2)^3 + 6\text{trex}^2 + 3\text{dex}[(\text{trex} - 1)^2 - 2] \in [-12, 36], \quad (44)$$

and

$$K_4 := (\text{dex} - 2)^2 + (\text{trex} - 1)^2 - 2 \in [0, 8]. \quad (45)$$

The minimum value of K_3 is reached for $\omega_1 = 1 = -\omega_2$ and $\omega_2 = 1 = -\omega_1$. For $\omega_1 = \omega_2 = -1$, $K_3 = 4$. The maximum value of K_3 is reached for $\omega_1 = \omega_2 = 1$. The minimum value of K_4 is reached for $\omega_1 = \omega_2 = 1$. The maximum value of K_4 is reached for $\omega_1 = \omega_2 = -1$, $\omega_1 = 1 = -\omega_2$ and $\omega_2 = 1 = -\omega_1$.

We analyze previous bounds for the values $\omega_i = \pm 1$, $i = 1, 2$, and in the cases $|\lambda\alpha_2| \gg 1$, $\lambda\alpha_2 \approx -1$ and $|\lambda\alpha_2| \ll 1$. The resulting sufficient conditions are (see Appendix B for more details):

$$\begin{aligned} -\frac{20}{9} &\leq c_1 - 4c_2 \leq 0, \quad -1 + 3(1 - 2c_1)(c_1 + 4c_2) \leq 0, \\ 0 &\leq 73 + 18c_1^2 - 180c_2 + 9c_1(3 + 8c_2), \quad 0 \leq 9c_1 - 12c_2 - 6c_1^2 - 24c_1c_2 + 143, \\ 0 &\leq 103 - 15c_1 - 6c_1^2 + 84c_2 - 24c_1c_2, \quad 0 \leq 6c_1^2 - 15c_1 + 36c_2 + 24c_1c_2 + 71, \end{aligned} \quad (46)$$

together with

$$\begin{aligned} \lambda\alpha_2(-1 + c_1 - 4c_2) &\leq \frac{8}{3}, \quad -24 \leq \lambda^2\alpha_2^2(c_1 - 4c_2), \\ \lambda^3\alpha_2^3[-1 + 3(1 - 2c_1)(c_1 + 4c_2)] &\leq 48. \end{aligned} \quad (47)$$

For $|\lambda\alpha_2| \ll 1$, first inequality in (47) is the most relevant one. Firstly, we minimize $|-1 + c_1 - 4c_2|$ (taking into account (46)). Consequently, we choose $c_2 = c_1/4$. This condition minimizes the factors accompanying $\lambda\alpha_2$ and $\lambda^2\alpha_2^2$ in (47). The remaining inequalities from (46) and (47) reduce to

$$\frac{3 - \sqrt{1245}}{12} \leq c_1 \leq \frac{3 + \sqrt{1245}}{12}, \quad \lambda^3\alpha_2^3(-1 + 6c_1 - 12c_1^2) \leq 48. \quad (48)$$

Secondly, we minimize $|-1 + 6c_1 - 12c_1^2|$ (taking into account its allowed range). The minimum is placed at $c_1 = 1/4$. Therefore, the resulting values are

$$(c_1, c_2) = \left(\frac{1}{4}, \frac{1}{16}\right), \quad (49)$$

and the method is written as

$$\begin{cases} u^{(1)} = u^n + \Delta t L_1(u^n, v^n), \\ v^{(1)} = v^n + \Delta t \left[\frac{3}{4}L_2(u^n) + \frac{1}{4}L_2(u^{(1)}) + L_3(u^n, v^n) \right], \end{cases} \quad (50)$$

$$\begin{cases} u^{(2)} = \frac{1}{4} \left[3u^n + u^{(1)} + \Delta t L_1(u^{(1)}, v^{(1)}) \right], \\ v^{(2)} = v^n + \frac{\Delta t}{4} \left[\frac{3}{4}L_2(u^n) + \frac{1}{4}L_2(u^{(1)}) + L_2(u^{(2)}) \right. \\ \left. + L_3(u^n, v^n) + L_3(u^{(1)}, v^{(1)}) \right], \end{cases} \quad (51)$$

$$\begin{cases} u^{n+1} = \frac{1}{3} \left[u^n + 2u^{(2)} + 2\Delta t L_1(u^{(2)}, v^{(2)}) \right], \\ v^{n+1} = v^n + \frac{\Delta t}{6} \left[L_2(u^n) + L_2(u^{(1)}) + 4L_2(u^{(2)}) \right. \\ \left. + L_3(u^n, v^n) + L_3(u^{(1)}, v^{(1)}) + 4L_3(u^{(2)}, v^{(2)}) \right]. \end{cases} \quad (52)$$

For $|\lambda\alpha_2| \gg 1$, last inequality in (47) is the most relevant one. Firstly, we minimize $|-1 + 3(1 - 2c_1)(c_1 + 4c_2)|$ (taking into account (46)). Consequently, we

choose $c_2 = \frac{1}{4} \left(\frac{1}{3(1-2c_1)} - c_1 \right)$. This condition minimizes the factor accompanying $\lambda^3 \alpha_2^3$ in (47). The remaining inequalities from (46) and (47) reduce to

$$\frac{-17 - \sqrt{2377}}{72} \leq c_1 \leq \frac{-17 + \sqrt{2377}}{72}, \quad (53)$$

and

$$\lambda \alpha_2 \left(-1 + \frac{(-1 + 6c_1 - 12c_1^2)}{3(2c_1 - 1)} \right) \leq \frac{8}{3}, \quad 24 \leq \lambda^2 \alpha_2^2 \frac{(-1 + 6c_1 - 12c_1^2)}{3(2c_1 - 1)}. \quad (54)$$

Secondly, we minimize $\left| \frac{(-1 + 6c_1 - 12c_1^2)}{3(2c_1 - 1)} \right|$ (taking into account its allowed range).

The minimum is placed at $c_1 = \frac{3 - \sqrt{3}}{6}$. Therefore, the resulting values are

$$(c_1, c_2) = \left(\frac{3 - \sqrt{3}}{6}, \frac{-1 + \sqrt{3}}{8} \right), \quad (55)$$

and the method is written as

$$\begin{cases} u^{(1)} = u^n + \Delta t L_1(u^n, v^n), \\ v^{(1)} = v^n + \Delta t \left[\frac{(3 + \sqrt{3})}{6} L_2(u^n) + \frac{(3 - \sqrt{3})}{6} L_2(u^{(1)}) + L_3(u^n, v^n) \right], \end{cases} \quad (56)$$

$$\begin{cases} u^{(2)} = \frac{1}{4} \left[3u^n + u^{(1)} + \Delta t L_1(u^{(1)}, v^{(1)}) \right], \\ v^{(2)} = v^n + \frac{\Delta t}{4} \left[\frac{(3 + \sqrt{3})}{6} L_2(u^n) + \frac{(-1 + \sqrt{3})}{2} L_2(u^{(1)}) + \frac{2}{3} (3 - \sqrt{3}) L_2(u^{(2)}) \right. \\ \left. + L_3(u^n, v^n) + L_3(u^{(1)}, v^{(1)}) \right], \end{cases} \quad (57)$$

$$\begin{cases} u^{n+1} = \frac{1}{3} \left[u^n + 2u^{(2)} + 2\Delta t L_1(u^{(2)}, v^{(2)}) \right], \\ v^{n+1} = v^n + \frac{\Delta t}{6} \left[L_2(u^n) + L_2(u^{(1)}) + 4L_2(u^{(2)}) \right. \\ \left. + L_3(u^n, v^n) + L_3(u^{(1)}, v^{(1)}) + 4L_3(u^{(2)}, v^{(2)}) \right]. \end{cases} \quad (58)$$

As in the second-order PIRK methods, depending of the value of $|\lambda \alpha_2| = |\bar{\lambda} \bar{\alpha}_2| \Delta t^2$, it will be more convenient to use a particular set of values for the coefficients. This fact will be illustrated in Sect. 4.

3.5 Comments on the PIRK methods and some IMEX ones

In this subsection we comment briefly on the derived PIRK methods, the second-order IMEX-SSP2(2,2,2) and third-order IMEX-SSP3(4,3,3) from [5].

The IMEX-SSP2(2,2,2) method particularized to the system (1) reads:

$$\begin{cases} u^{(1)} = u^n, \\ v^{(1)} = v^n + \Delta t L_2(u^n), \end{cases} \quad (59)$$

$$\begin{cases} u^{(2)} = u^n + \Delta t L_1(u^{(1)}, v^{(1)}), \\ v^{(2)} = v^n + \Delta t \left[(1 - 2\gamma)L_2(u^n) + \gamma L_2(u^{(2)}) + L_3(u^{(1)}, v^{(1)}) \right], \end{cases} \quad (60)$$

$$\begin{cases} u^{n+1} = u^n + 0.5\Delta t \left[L_1(u^{(1)}, v^{(1)}) + L_1(u^{(2)}, v^{(2)}) \right], \\ v^{n+1} = v^n + 0.5\Delta t \left[L_2(u^n) + L_2(u^{(2)}) + L_3(u^{(1)}, v^{(1)}) + L_3(u^{(2)}, v^{(2)}) \right], \end{cases} \quad (61)$$

where $\gamma = 1 - 1/\sqrt{2}$. The IMEX-SSP2(2,2,2) method is L-stable, and, in comparison with the both derived second-order PIRK methods, there is an additional intermediate stage. On one hand, the second-order PIRK methods provide a stable evolution for a wave equation in spherical-type coordinates as it is shown in Sect. 4. On the other hand, the evolution of a wave-like equation with extra complex non-linear source terms using a numerical scheme with an extra stage is translated into extra computational costs.

The IMEX-SSP3(4,3,3) method particularized to the system (1) reads:

$$\begin{cases} u^{(1)} = u^n, \\ v^{(1)} = v^n + \Delta t L_2(u^n), \end{cases} \quad (62)$$

$$\begin{cases} u^{(2)} = u^n, \\ v^{(2)} = v^n, \end{cases} \quad (63)$$

$$\begin{cases} u^{(3)} = u^n + \Delta t L_1(u^n, v^n), \\ v^{(3)} = v^n + \Delta t \left[(1 - \alpha)L_2(u^n) + \alpha L_2(u^{(3)}) + L_3(u^n, v^n) \right], \end{cases} \quad (64)$$

$$\begin{cases} u^{(4)} = u^n + 0.25 \Delta t \left[L_1(u^n, v^n) + L_1(u^{(3)}, v^{(3)}) \right], \\ v^{(4)} = v^n + \Delta t \left[\beta L_2(u^n) + (0.5 - \alpha - \beta)L_2(u^{(3)}) + \alpha L_2(u^{(4)}) \right. \\ \left. + 0.25 L_3(u^n, v^n) + 0.25 L_3(u^{(3)}, v^{(3)}) \right], \end{cases} \quad (65)$$

$$\begin{cases} u^{n+1} = u^n + \frac{\Delta t}{6} \left[L_1(u^n, v^n) + L_1(u^{(3)}, v^{(3)}) + 4L_1(u^{(4)}, v^{(4)}) \right], \\ v^{n+1} = v^n + \frac{\Delta t}{6} \left[L_2(u^n) + L_2(u^{(3)}) + 4L_2(u^{(4)}) \right. \\ \left. + L_3(u^n, v^n) + L_3(u^{(3)}, v^{(3)}) + 4L_3(u^{(4)}, v^{(4)}) \right], \end{cases} \quad (66)$$

where $\alpha = 0.24169426078821$, $\beta = 0.18957643480295$. Due to the particular structure of the system (1), the resulting two first stages can be omitted, and the final number of stages is similar to the case of third-order PIRK methods. The trivial value for $v^{(2)}$ results from a cancellation, as a consequence of the presence of opposite coefficients in the numerical scheme. Notice that negative coefficients are avoided in the derivation of the PIRK methods.

The IMEX-SSP3(4,3,3) method corresponds to a third-order PIRK one, with $c_1 = \alpha = 0.24169426078821$ and $c_2 = (1 - 3c_1)/4 = 0.06872930440884$. These values for the coefficients are close to one of the optimal sets deduced in Sect. 3.4, $c_1 = 4c_2 = 1/4$.

4 Numerical experiments

In this section, the PIRK methods described in Sect. 3 are applied to the case of the time evolution of a wave equation for a scalar, h , in spherical coordinates. A wave equation for h can be written as:

$$\partial_{tt}h = \Delta h, \quad (67)$$

where Δ is the Laplacian operator. Eq. (67) can be rewritten as a first-order system in time, with the addition of an extra auxiliary variable, A , as follows:

$$\begin{aligned} \partial_t h &= A, \\ \partial_t A &= \Delta h. \end{aligned} \quad (68)$$

In this case, according to system (1), the variables can be identified as $(u, v) = (h, A)$, and the operators as $\mathcal{L}_1(h, A) = A$, $\mathcal{L}_2(h) = \Delta h$ and $\mathcal{L}_3(h, A) = 0$. Therefore, $\bar{\alpha}_1 = \bar{\gamma}_1 = \bar{\gamma}_2 = 0$ and $\bar{\alpha}_2 = 1$ in system (11). The eigenvalues of the linearized explicit part are $\omega_1 = \omega_2 = 1$ and hence $\text{dex} = 1$ and $\text{trex} = 2$. $\bar{\lambda} \in \mathbb{R}^-$ and its value depends on the particular solution for h and the discretization of the operator Δ . Spherical coordinates are used, being $\left(\frac{\partial}{\partial r}, \frac{1}{r} \frac{\partial}{\partial \theta}, \frac{1}{r \sin \theta} \frac{\partial}{\partial \varphi}\right)$ the corresponding orthonormal basis.

Eq. (67) has solutions of the form

$$h(r, \theta, \varphi, t) \sim j_l(kr) Y_{lm}(\theta, \varphi) \cos kt, \quad (69)$$

being j_l the spherical Bessel function of first kind of order l and Y_{lm} the spherical harmonics. The value of k , a positive real constant, is determined by imposing boundary conditions. We search for solutions inside a sphere of radius unity imposing $h(r = 1, \theta, \varphi, t) = 0$. For fixed l and m it is possible to compute the eigenmode frequencies, k_{nl} , as the zeros of the spherical Bessel function of order l , being $n = 1$ the first zero and so on.

We have performed 1D-spherical, 2D-axisymmetric and 3D simulations of the system using as initial data solutions with $n = 1$ at $t = 0$. We use values of (l, m) equal to $(0, 0)$, $(2, 0)$ and $(2, 2)$ for the 1D, 2D and 3D case, respectively. In this way, the initial data is regular and fulfills the symmetries in each case. Furthermore, the data is non trivial for each symmetry in the sense that there are not trivial cancellations for 2D and 3D simulations. We consider symmetry with respect to the equatorial plane, $\theta = \pi/2$.

We use a finite difference scheme to solve the system using an equally-spaced grid with n_r , n_θ and n_φ grid points in the r , θ and φ directions, respectively. We use derivatives of cell-centered Lagrange interpolation polynomials [12] to compute the first and second spatial derivatives appearing in the Laplacian operator, achieving fourth, sixth and eighth discretization order. Boundary conditions are imposed by using a number of ghost cells consistent with the discretization stencil. At $r = 1$ the analytical solution is imposed as boundary condition. At all other boundaries symmetry conditions are used. The maximum time step is determined by the CFL condition for the speed of the wave, which is 1. The time step in the simulations is a fraction smaller than the maximum time step, the CFL factor, in the interval $[0, 1]$.

We can estimate the absolute error of the numerical evolution by comparing the numerical solution with the analytical one given by Eq. (69). As a measure of the global error during the numerical evolution, we compute the L_2 -norm of the difference between the numerical and the analytical solutions at a given time,

$$L_2(h)(t) = \frac{1}{n_r n_\theta n_\varphi} \sqrt{\sum_{r,\theta,\varphi} [h_{\text{num}}(r, \theta, \varphi, t) - h_{\text{ana}}(r, \theta, \varphi, t)]^2 (kr)^2}. \quad (70)$$

4.1 Stability

We have studied numerically the stability of the first, second and third-order PIRK methods. This study involves the numerical computation of a wide parameter space, including the coefficients c_i of the PIRK methods and the CFL factor. Up to 10000 simulations have to be performed to cover this parameter space, so we have decided to use a single numerical setup as reference for the stability study. We use $(n, l, m) = (1, 2, 0)$ for the initial data in 2D-axisymmetry with equatorial symmetry. In this case, $k_{12} \approx 5.763$. We use $(n_r, n_\theta) = (100, 32)$ grid points and a fourth-order spatial discretization scheme.

With the numerical setup fixed, we can estimate the value of $x := -\lambda\alpha_2 = -\bar{\lambda}(\Delta t)^2$, which is the relevant quantity for the stability of the system. For solutions of the form (69), Eq. (68) can be written as

$$\begin{aligned} \partial_t h &= A, \\ \partial_t A &= -k^2 h. \end{aligned} \quad (71)$$

Therefore, $\bar{\lambda} = -k^2$. The minimum value of k corresponds to the fundamental mode $(n, l, m) = (1, 0, 0)$, i.e. $k_{\min} = k_{10} = \pi$. This sets the lower limit for x ,

$$x_{\min} = \pi^2 (\Delta t)^2. \quad (72)$$

Note that in the limit of infinite resolution, the CFL restriction results in $\Delta t \rightarrow 0$ and $x_{\min} \rightarrow 0$. We show in the next subsections that this is indeed the case for the typical resolutions used in practical applications.

The maximum value of k corresponds to solutions with typical spatial variations of the order of the smallest grid cell size, Δl_{\min} . For these solutions,

$$k_{\max} \approx \frac{2\pi}{\Delta l_{\min}}, \quad (73)$$

and hence the upper limit for x is

$$x_{\max} = k_{\max}^2 (\Delta t)^2 \approx \left(\frac{2\pi \Delta t_{\max}}{\Delta l_{\min}} \right)^2 (\text{CFL factor})^2 = 4\pi^2 (\text{CFL factor})^2, \quad (74)$$

being the CFL factor = $\Delta t / \Delta t_{\max}$ and $\Delta t_{\max} = \Delta l_{\min}$ the maximum time step allowed by the CFL condition, which coincides with the smallest grid cell size. Note that x_{\max} does not depend on the resolution. As a consequence, the stability properties of the system do not depend on the resolution, but only on the CFL factor. For convenience we define $\bar{x} := x / (\text{CFL factor})^2$; therefore, $\bar{x}_{\min} = \pi^2 (\Delta t_{\max})^2$ and $\bar{x}_{\max} = 4\pi^2$. By keeping the numerical setup fixed, we expect that the limits of \bar{x}

stay constant in all our simulations. Effects of the dimensionality and resolution are discussed in section 5.

For each order of the PIRK methods, we compare stability behavior of the numerical simulations with the stability criterion of Sect. 3 for the determinant of the corresponding matrix of a given method. We compare this stability criterion with the general one for the eigenvalues of the system.

4.1.1 First-order method

The expression for $\det(M_1)$ particularized to the system (68) with $x > 0$, is

$$\det M_1 = 1 + (1 - c_1)x, \quad (75)$$

and the eigenvalues of M_1 are

$$e_{\pm} = \frac{1}{2} \left(2 - c_1x \pm \sqrt{-x(4 - c_1^2x)} \right). \quad (76)$$

The stability criterion, $|e_{\pm}| \leq 1$, for $x \neq 0$, results in

$$1 \leq c_1 \leq \frac{1}{2} + \frac{2}{x}, \quad (77)$$

$$x \leq 4. \quad (78)$$

The condition $|\det M_1| \leq 1$, used in Sect. 3, results in

$$1 \leq c_1 \leq 1 + \frac{2}{x}, \quad (79)$$

which is a necessary, but not sufficient, condition for stability. Conditions (77)–(79) are more restrictive for larger values of x , so the value \bar{x}_{\max} determines the stability properties of the system.

It is therefore relevant to study the stability properties of the numerical solution depending on the coefficient c_1 and the time step Δt . We have performed series of simulations for several CFL factors (0.3, 0.4, 0.5, 0.6, 0.7, 0.8, 0.85 and 0.9), varying the value of c_1 from 0 to 5 in steps of 0.001. We have evolved each simulation up to time $t = 54$, i.e. about 50 oscillations. The left panel of Fig. 1 shows the evolution of the L_2 -norm for a selection of simulations. The behavior of this quantity allows us to distinguish between numerically stable and unstable evolutions. Numerically stable evolutions (solid lines) show an oscillatory behavior of the L_2 -norm with values smaller than one, while numerically unstable evolutions (dashed lines) show an exponential grow of the L_2 -norm which becomes much larger than 1. Hereafter, we define numerical stability for our numerical simulations as those in which L_2 -norm < 1 for a time corresponding to 50 oscillations, i.e. $t = 100\pi/\omega$.

For each CFL factor, we find a maximum and minimum values of c_1 such that all simulations within this two values are numerically stable, while lower or higher values lead to numerically unstable evolutions. No numerically stable values of c_1 were found for a CFL = 0.9. The right panel of Fig. 1 shows the stability limits (red and black circles). We can compare these limits with the predictions of Eqs. (77) and (78). For all CFL factors the lower limit is $c_1 = 1$ and coincides with the prediction of Eq. (77). Following Eq. (77), we fit the upper bound by a curve of the form $p_1 + p_2(\Delta t_{\max}/\Delta t)^2$, with $p_1 = 0.501$, $p_2 = 0.3746$ and Δt_{\max}

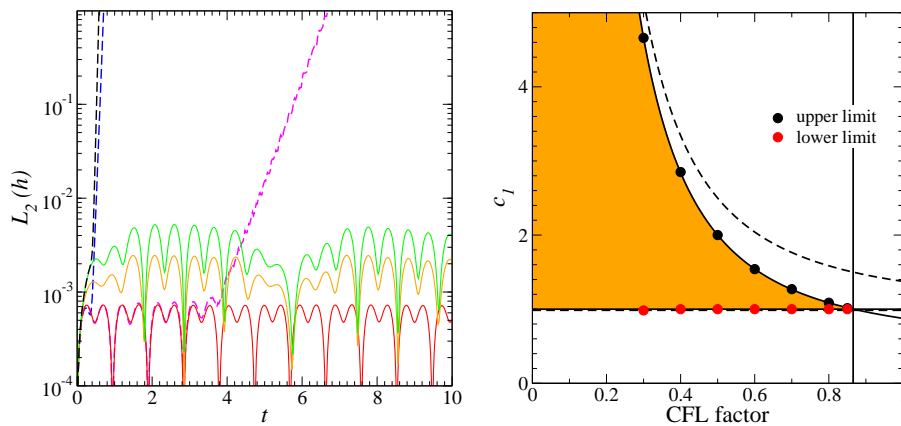


Fig. 1 Stability of the first-order PIRK method. *Left panel:* time evolution of the L_2 -norm for simulations with CFL factor 0.5 and c_1 values of 0.9 (blue), 0.99 (magenta), 1 (red), 1.5 (orange), 2 (green) and 2.05 (black). Solid and dashed lines represent numerically stable and unstable simulations, respectively. *Right panel:* stability region depending on the values for c_1 and the CFL factor. Red and black circles are the maximum and minimum values of c_1 , respectively, for which a numerically stable evolution is found for each CFL factor. Solid lines are the boundaries of the stability region (orange area) given by Eqs. (77) and (78), for the fitted value of $\bar{x} = 5.340$. The boundary of the region $|\det(M_1)| \leq 1$, which partially coincides with the stability boundaries, is also plotted (dashed lines).

the maximum time step predicted by the CFL condition. We confirm the $1/(\Delta t)^2$ behavior of the upper limit and a value of p_1 compatible with the predicted $1/2$ in Eq. (77). From the fitted value of p_2 we estimate $\bar{x} = 5.340$, which is of the order of magnitude of $\bar{x}_{\max} \approx \pi^2$. Using this estimation for \bar{x} , it is possible to compute the maximum CFL factor using the condition (78). It results to be 0.8656, consistent with not finding any stable simulation for CFL = 0.9.

If we consider the stability criterion used in section 3.2 (dashed-line in Fig. 1) for the determinant of M_1 , we observe that this criterion is overestimating the stability region. However, the estimated optimal value, $c_1 = 1$, lays inside the stability region and is indeed the value such that the maximum CFL factor is achievable.

The first-order ERK can be recovered by setting $c_1 = 0$ ¹. Since none of our numerical simulations with $c_1 = 0$ and CFL factors between 0.3 and 0.95 show stable evolutions (see right panel of Fig. 1), we have performed simulations decreasing the CFL factor to try to find the stability limit. We were not able to find stable evolutions for CFL factors as low as 0.001. The reason for this behavior is that the eigenvalues of the first-order ERK, given by Eq. (76) with $c_1 = 0$, read

$$e_{\pm} = 1 \pm \sqrt{-x}, \quad (80)$$

and the stability criterion, $|e_{\pm}| \leq 1$, is only fulfilled for $x = 0$, i.e. $\Delta t = 0$. If we decrease the CFL factor, i.e. approach $|e_{\pm}| = 1$, the instability appears at later time in the simulation (e.g., for CFL = 0.001 the instability appears at $t \sim 7$). The

¹ Alternatively, identical result can be obtained by setting $\bar{\alpha}_1 = \bar{\gamma}_1 = \bar{\lambda} = 0$, $\bar{\alpha}_2 = 1$ and $\bar{\gamma}_1 \neq 0$ for all of the PIRK methods presented in this work.

consequence is that first-order ERK can be used for finite-time evolutions provided a sufficiently small CFL factor is used. However, the time step restriction of the first-order ERK is significantly larger (several orders of magnitude) than the one of the first-order PIRK.

4.1.2 Second-order method

The expression for $\det(M_2)$ particularized to the system (68) with $x > 0$, is

$$\det(M_2) = \frac{1}{4} [4 - x(2c_2 - c_1 - 2c_1c_2)], \quad (81)$$

and the eigenvalues of M_2 are

$$e_{\pm} = 1 - \frac{x}{2} + \frac{c_1}{8}(1 - 2c_2)x^2 \pm \frac{1}{8} \sqrt{-x[64 - 16(1 + 2c_1 - 2c_2)x + 8c_1(1 - 2c_2)x^2 - c_1^2(1 - 2c_2)^2x^3]}. \quad (82)$$

The stability condition, $|e_{\pm}| \leq 1$, leads to

$$\frac{4}{x} \left(1 - \frac{4}{x}\right) \leq c_1(1 - 2c_2) \leq \frac{4}{x}, \quad (83)$$

$$c_1 - c_2 \leq 2/x, \quad (84)$$

$$c_2(2c_1 - 1) \leq \frac{2}{x} \left(-1 + \frac{4}{x}\right), \quad (85)$$

$$0 \leq c_1 + 2c_2(c_1 - 1). \quad (86)$$

The condition $|\det(M_2)| \leq 1$ is equivalent to

$$0 \leq c_1 + 2c_2(c_1 - 1) \leq \frac{8}{x^2}, \quad (87)$$

which coincides partially with the boundaries of the stability region. The conditions (83)-(86) and (87) are more restrictive for larger values of x , therefore the value \bar{x}_{\max} determines the stability properties of the system.

We have studied the numerical stability of the second-order PIRK by performing simulations using $c_1 \in [-0.5, 1.5]$ and $c_2 \in [-0.5, 1.5]$, varying the coefficients in steps of 0.02. We have used several CFL values (0.5, 0.7, 0.8 and 0.9). Fig. 2 shows the stability region on the (c_1, c_2) plane. According to Eqs. (83)-(86), the boundaries of the stability region depend only on the parameter \bar{x} . In order to estimate \bar{x} , we perform a χ^2 -minimization of the difference between the numerically determined boundaries for all CFL factors and the theoretically predicted values. We obtain $\bar{x} = 5.373$ with high significance ($\chi^2 = 353.7$ for 385 degrees of freedom). Note that, as expected, the value of \bar{x} is very close to the one obtained in the first-order PIRK method. The boundaries for the fitted value of \bar{x} (solid-lines in Fig. 2) agree very closely with the numerically computed ones. As in the first-order PIRK, the criterion $|\det M_2| \leq 1$ overestimates the stability region (dashed-lines in Fig. 2).

We can compare the numerical results for the stability region with the optimal values computed in Sect. 3.3: $(c_1, c_2) = (1/2, 0)$ for $|x| \ll 1$ (black circle in Fig. 2) and $(c_1, c_2) = \frac{1}{2}(2 - \sqrt{2}, \sqrt{2} - 1)$ for $|x| \gg 1$ (star symbol in Fig. 2). Both values

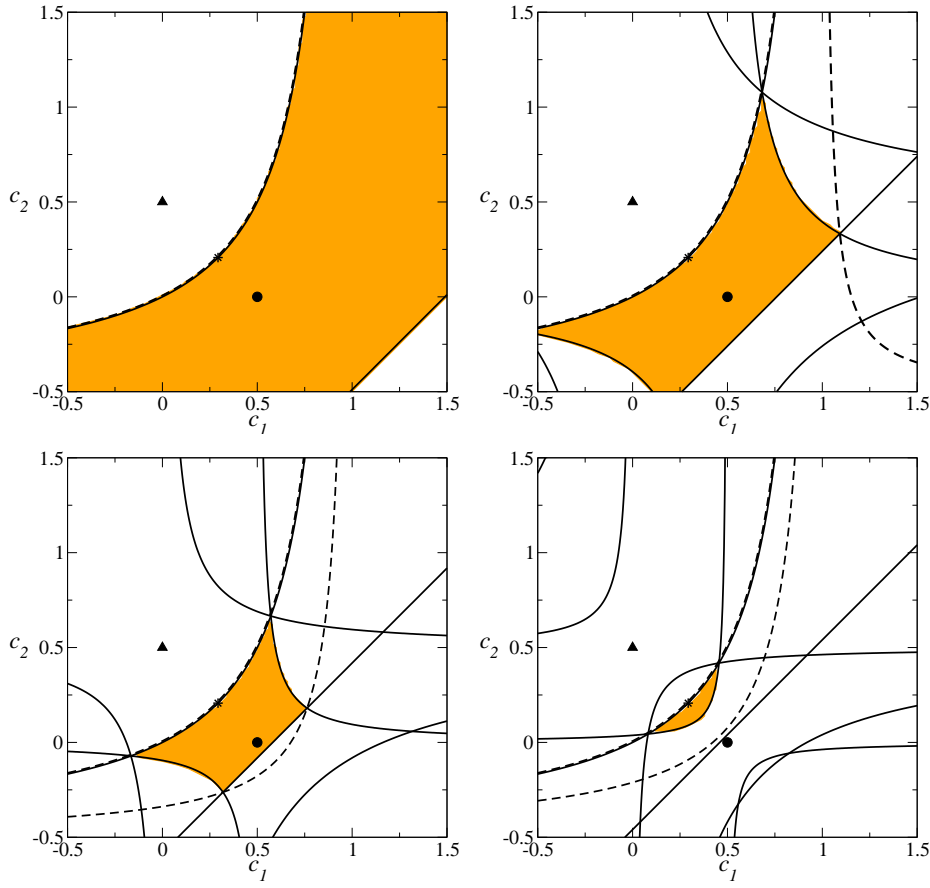


Fig. 2 Dependence of the numerically determined stability region (orange area) on the (c_1, c_2) coefficients for the evolution of h using a second-order PIRK method. The boundaries (solid lines) of the stability region according to Eqs. (83)-(86) for $\bar{x} = 5.373$, and the boundaries (dashed lines) of the region $|\det(M_2)| \leq 1$, which partially coincide with the stability boundaries, are plotted. The values for the optimal second-order PIRK method with $(c_1, c_2) = (1/2, 0)$ (black circle) and $(c_1, c_2) = 1/2(2 - \sqrt{2}, \sqrt{2} - 1)$ (star symbol), and the second-order ERK (black triangle) are also plotted.

allow for stable numerical evolutions with CFL factors close to unity. According to the fit, $x = 5.373$ (CFL factor)², which is larger than unity for CFL factors larger than 0.434. Indeed, the choice $(c_1, c_2) = \frac{1}{2}(2 - \sqrt{2}, \sqrt{2} - 1)$ is better suited for higher CFL values, while the choice $(c_1, c_2) = (1/2, 0)$ becomes unstable. Therefore, we recommend the optimal values $(c_1, c_2) = \frac{1}{2}(2 - \sqrt{2}, \sqrt{2} - 1)$ as they seem to provide stable evolutions with the largest possible CFL factors.

The second-order ERK correspond to the case $(c_1, c_2) = (0, 1/2)$ and is unconditionally unstable. In this case, the eigenvalues are

$$e_{\pm} = 1 - \frac{x}{2} \pm \sqrt{-x}, \quad (88)$$

and the stability criterion, $|e_{\pm}| \leq 1$, is only fulfilled for $\Delta t = 0$. Therefore, the observed numerical behavior of the second-order ERK is very similar to the first-order ERK.

4.1.3 Third-order method

The expression for $\det(M_3)$ particularized to the system (68) with $x > 0$ is

$$\det(M_3) = 1 + \frac{x^2}{12}(c_1 - 4c_2) + \frac{x^3}{72}[-1 + 3(1 - 2c_1)(c_1 + 4c_2)], \quad (89)$$

and the eigenvalues of M_3 are

$$e_{\pm} = 1 - \frac{x}{2} + \frac{x^2}{24}(1 + c_1 - 4c_2) - \frac{\sqrt{x}}{24} [192(x - 3) - 16x^2(3c_1(1 - c_1 - 4c_2) + 1) + x^3(1 + c_1 - 4c_2)^2]^{1/2}. \quad (90)$$

The stability criterion, $|e_{\pm}| \leq 1$, for $x \neq 0$ results in

$$\frac{12}{x} \left(1 - \frac{4}{x}\right) \leq 1 + c_1 - 4c_2 \leq \frac{12}{x}, \quad (91)$$

$$1 + 3(2c_1 - 1)(c_1 + 4c_2) \leq \frac{6}{x} \left(\frac{12}{x} - 1\right), \quad (92)$$

$$1 + 3(2c_1 - 1)(c_1 + 4c_2) \leq \frac{6}{x} \left[\frac{12}{x} \left(\frac{4}{x} - 1\right) - 1 + 2(1 + c_1 - 4c_2)\right], \quad (93)$$

$$\frac{6}{x}(c_1 - 4c_2) \leq 1 + 3(2c_1 - 1)(c_1 + 4c_2). \quad (94)$$

The condition $|\det(M_3)| \leq 1$ is equivalent to

$$\frac{6}{x}(c_1 - 4c_2) \leq 1 + 3(2c_1 - 1)(c_1 + 4c_2), \quad (95)$$

$$-144 \leq 6x^2(c_1 - 4c_2) + x^3[-1 + 3(1 - 2c_1)(c_1 + 4c_2)], \quad (96)$$

which coincides partially with the boundaries of the stability region. The conditions (91)-(93) and (96) are more restrictive for larger values of x , therefore the value \bar{x}_{\max} determines the stability properties of the system at these boundaries. However the condition (94) (which is equivalent to (95)), can be more restrictive for small values of x depending on the value of c_1 and c_2 . For this case, both \bar{x}_{\max} and \bar{x}_{\min} are relevant for the analysis of the stability.

We have performed the same numerical stability analysis for the third-order PIRK as in Sect. 4.1.2. The numerically computed stability regions depending on (c_1, c_2) are shown in Fig. 3 for different CFL factors. As in the second-order method, the stability regions shrinks for increasing CFL factors. We have performed a χ^2 minimization to determine the value of \bar{x} which fits better the boundaries of the stability region with the expressions (91)-(94). We obtain $\bar{x} = 5.322$ ($\chi^2 = 109.0$ for 255 degrees of freedom). For the numerical setup considered, we estimate $\bar{x}_{\min} = 6.945 \times 10^{-7} \ll 1$, so we consider as a boundary the condition (94) setting $x = 0$ (brown solid line in Fig. 3). The resulting boundaries (solid lines in Fig. 3) fit very well with the numerically estimated stability region

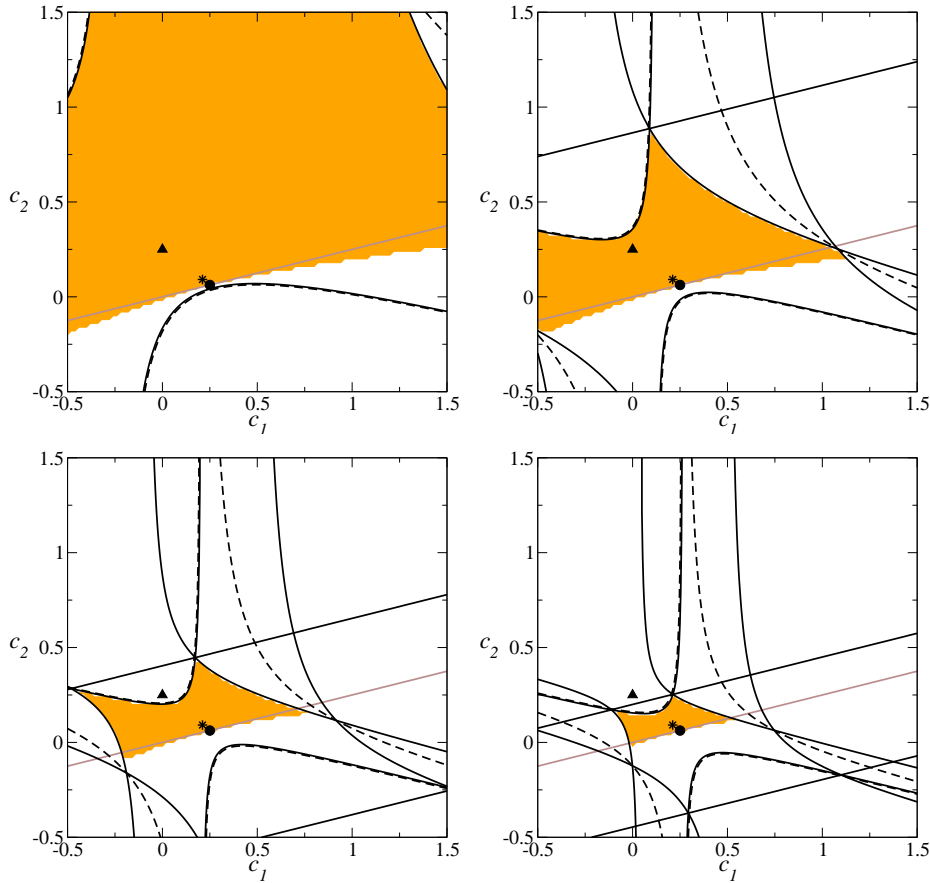


Fig. 3 Dependence of the numerically determined stability region (orange area) on the (c_1, c_2) coefficients for the evolution of h using a third-order PIRK method. The boundaries (solid lines) of the stability region according to Eqs. (91)-(94) for $\bar{x} = 5.322$ (black lines) and $\bar{x} = 0$ (brown line), and the boundaries of the region $|\det(M_3)| \leq 1$, which partially coincide with the stability boundaries, are plotted. The values for the optimal third-order PIRK methods, $(c_1, c_2) = (1/4, 1/16)$ (black circle) and $(c_1, c_2) = ((3 - \sqrt{3})/6, (-1 + \sqrt{3})/8)$ (star symbol), and the third-order ERK (black triangle), are also plotted.

(orange area in Fig. 3). The condition $|\det M_3| \leq 1$ (dashed lines in Fig 3) overestimate the stability region; however, the optimal values obtained in Sect. 3.4 (black circle and star symbol in Fig. 3) lay inside the stability region for all CFL factors studied. Since both values are very close, any of them could be used in the case of the wave equation for CFL factors close to unity. If we compare to the third-order IMEX-SSP3(4,3,3) in [5], corresponding to $c_1 = 0.24169426078821$ and $c_2 = (1 - 3c_1)/4 = 0.06872930440884$, the stability properties are very similar since the coefficients are very close to the optimal PIRK values, and therefore the method is numerically stable for the considered CFL factors.

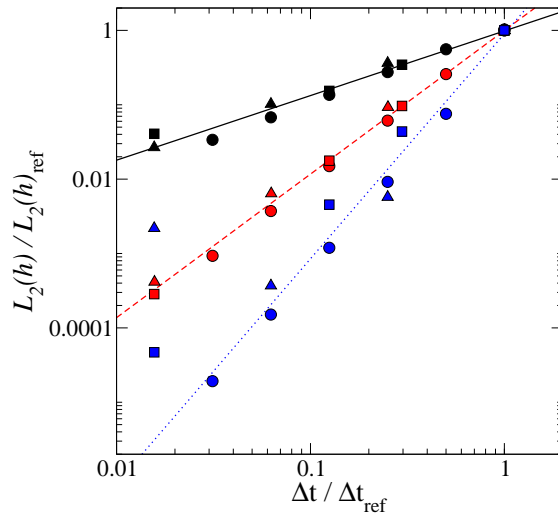


Fig. 4 Numerical error estimation for series of 1D (circles), 2D (triangles) and 3D (squares) simulations, normalized to the reference resolution of each series, as a function of the time step. Results for the first-order (black symbols), second-order (red symbols) and third-order (blue symbols) PIRK methods are shown. Black-solid line, red-dashed line and blue-dotted line correspond to power law fits for first-order, second-order and third-order PIRK respectively.

The third-order ERK corresponds to $(c_1, c_2) = (0, 1/4)$ (black triangle in Fig. 3). The eigenvalues of M_3 in this particular case are

$$e_{\pm} = 1 - \frac{x}{2} \pm \frac{1}{6} \sqrt{-x(x-6)^2}. \quad (97)$$

The condition $|e_{\pm}| \leq 1$ results in

$$0 \leq x \leq 3. \quad (98)$$

For the fitted value of \bar{x} , this condition restricts the stability of the third-order ERK to $\text{CFL} < 0.751$. Accordingly, our numerical simulations show numerical stability for 0.5 and 0.7 CFL factors, but not for 0.8 and 0.9. We conclude that, although the third-order ERK is stable, the time step is more restricted as in the third-order PIRK.

4.2 Convergence

We have studied the convergence properties of the PIRK methods by performing series of 1D-spherically symmetric, 2D-axisymmetric and 3D simulations. In each one, we use reference models with resolutions $n_r = 50$, $(n_r, n_{\theta}) = (50, 16)$ and $(n_r, n_{\theta}, n_{\varphi}) = (50, 8, 32)$, respectively. We increase the resolutions in all directions by the following factors: 2, 4, 8, 16 and 32 (1D); 2, 4, 8 (2D); 1.5, 2, 4 (3D). The L_2 -norm of h after $1/4$ period of oscillations, $t = \pi/\omega/2$, is used as an estimation of the error. To ensure that we measure the error due to the time discretization and not due to the spatial one, we choose the spatial order carefully. The time

step in 1D, 2D and 3D simulations in spherical coordinates scales as $\Delta t_{1D} \sim \Delta r$, $\Delta t_{2D} \sim \Delta r \Delta \theta$, and $\Delta t_{3D} \sim \Delta r \Delta \theta \Delta \varphi$, respectively, i.e., if we increase the resolution in all directions by a factor 2, Δt decreases in a factor 2, 4 and 8, respectively. Therefore, to ensure that increasing resolution the spatial discretization errors decrease faster than the time discretization errors, we choose fourth-order spatial discretization for the first-order PIRK, fourth-order (1D) and sixth-order (2D, 3D) for the second-order PIRK, and fourth-order (1D) and eighth-order (2D, 3D) for the third-order PIRK. In all cases, CFL = 0.8.

Fig. 4 shows the error, normalized to the error of the reference simulation of each series, as a function of the time step. Independently of the dimensionality of the simulation, the error falls with decreasing time step as expected from the convergence order of the PIRK used. Fitting to a power law, the convergence orders obtained are 0.87, 1.93 and 3.02 for first, second and third-order PIRK methods, respectively, very close to the expected ones. Note that for the 2D and 3D simulations using the third-order PIRK with highest resolution, the non-rescaled value of the L_2 -norm is close to 10^{-14} and its value is limited by the machine accuracy. These two points are not converging anymore and we do not consider them to compute the convergence order.

5 Conclusions

In this work, PIRK methods, from first to third-order of convergence, have been derived to evolve in time systems of non-linear partial differential equations containing stiff source terms. The origin of the stiffness can be due to a particular choice of coordinates; in the case of spherical coordinates, $1/r$ and $1/\sin\theta$ factors appear in the equations and can be interpreted numerically as stiff terms close to $r = 0$ and $\theta = 0, \pi$. Optimal SSP ERK methods are recovered when implicitly treated parts are neglected. The optimal values of the remaining coefficients are chosen according to stability criteria. Although the partially implicit parts confer stability to the system, no analytical or numerical inversion of any operator is required, and the computational costs of the derived PIRK methods are comparable to those of ERK ones.

We have applied the derived PIRK methods to the evolution of a scalar-wave equation and studied the numerical stability of the system depending on the coefficients of the PIRK methods and the CFL factor. We were able to explain the boundaries of the stability region by using the bound on the eigenvalues of the system, $|e_{\pm}| \leq 1$. The condition for the determinant, $|\det M| \leq 1$, which was used to optimize the coefficients of the methods in the first part of the present work, overestimates the size of the stability region. However, in all cases, the optimal values lay inside the stability region, and correspond to values for which the maximum CFL factors can be achieved. Therefore, although results of the study of this particular system cannot be extrapolated to a general case, we think that this behavior could be similar for other systems of equations, and the optimal values obtained here can be used in more general applications with similar performance.

The stability region of the methods can be determined in terms of the variable \bar{x} . This value does not depend on the particular resolution of the system and can be used to check consistency of the derivation of the methods. We have determined the value of the upper limit of \bar{x} for a set of 2D simulations with the same numerical

resolution and spatial discretization order. In all cases this value is very similar: 5.340, 5.373 and 5.322 for first, second and third-order PIRK methods, respectively. These values are consistent with the growth of modes with spatial-scales of order the smallest grid cell size. In the third-order PIRK method, we were able to confirm that the lower limit of \bar{x} is close to 0, as expected for the fundamental mode. Finally, we have checked the convergence order of our optimal PIRK methods, in agreement with the expected ones, in 1D-spherical, 2D-axisymmetric and 3D simulations.

Optimal SSP ERK methods can be viewed as particular cases for some values of the coefficients. First and second-order ERK result to be unconditionally unstable in both the linear stability analysis and the numerical simulations. The third-order ERK is stable, but the maximum CFL factor achievable is lower (0.751) than in the corresponding third-order PIRK (> 0.9). We suspect that the success of ERK methods in other works applied to wave-like equations could be due to the wide spread use of numerical-dissipation terms (e.g. [13]), which could avoid the growth of small-scale unstable modes. Our numerical method does not need these numerical-dissipation terms to get stable evolutions. We have observed similar performance in the comparison of the second and third-order PIRK methods with the IMEX-SSP2(2,2,2) and IMEX-SSP3(4,3,3) of [5], respectively. Regarding the second-order methods, the PIRK needs one stage less, which can be an advantage concerning the computational costs. Regarding the third-order methods, we have checked that the two first stages of the IMEX-SSP3(4,3,3) are redundant and this method corresponds to a PIRK one with coefficient values very close to the optimal ones derived in this work.

These methods are also appropriate to evolve generalized complex wave equations in spherical coordinates, as it has been shown in a recent application [14] for the evolution of Einstein equations in a particular formulation [15] using spherical orthonormal coordinates. The results of using these numerical schemes to evolve other systems of equations have to be explored, but this is beyond the scope of this work.

A Stability conditions for second-order PIRK methods

In this appendix we detail the derivation of the inequalities (29) and (30). We would like to guarantee

$$-4 \leq K_1 + \lambda\alpha_2 K_2(1 - 2c_1 + 2c_2) + \lambda^2\alpha_2^2(2c_2 - c_1 - 2c_1c_2) \leq 4, \quad (99)$$

for $\omega_i = 0, \pm 1$, $i = 1, 2$, and in the cases $|\lambda\alpha_2| \gg 1$, $\lambda\alpha_2 \approx -1$ and $|\lambda\alpha_2| \ll 1$:

1. Upper bound, $\omega_1 = \omega_2 = \pm 1$: $K_1 = 4$, $K_2 = 0$. In all the cases we require $2c_2(1 - c_1) - c_1 \leq 0$.
2. Upper bound, $\omega_1 = -\omega_2 = -\pm 1$: $K_1 = 4$, $K_2 = 2$.
For $|\lambda\alpha_2| \ll 1$, we require $0 \leq 1 - 2c_1 + 2c_2$. This condition is sufficient for the cases $|\lambda\alpha_2| \gg 1$ and $\lambda\alpha_2 \approx -1$.
3. Upper bound, $\omega_1 = \omega_2 = 0$: $K_1 = 1$, $K_2 = 1$. Previous derived conditions are sufficient for all the cases.
4. Lower bound, $\omega_1 = \omega_2 = \pm 1$: $K_1 = 4$, $K_2 = 0$. In all the cases we require $-8 \leq \lambda^2\alpha_2^2(2c_2 - c_1 - 2c_1c_2)$. This condition will be satisfied by the following ones.
5. Lower bound, $\omega_1 = -\omega_2 = -\pm 1$: $K_1 = 4$, $K_2 = 2$.
For $|\lambda\alpha_2| \ll 1$, we require $-4 \leq \lambda\alpha_2(1 - 2c_1 + 2c_2)$.
For $|\lambda\alpha_2| \gg 1$, previous derived conditions are sufficient.
For $\lambda\alpha_2 \approx -1$, we require $0 \leq 6 + 5c_1 - 6c_2 + 2c_1c_2$.

6. Lower bound, $\omega_1 = \omega_2 = 0$: $K_1 = 1$, $K_2 = 1$.
 For $|\lambda\alpha_2| \ll 1$, previous derived conditions are sufficient.
 For $|\lambda\alpha_2| \gg 1$, we require $-5 \leq \lambda^2\alpha_2^2(2c_2 - c_1 - 2c_1c_2)$.
 For $\lambda\alpha_2 \approx -1$, we require $0 \leq 4 + c_1 - 2c_1c_2$.

B Stability conditions for third-order PIRK methods

In this appendix we detail the derivation of the inequalities (46) and (47). We would like to guarantee

$$\begin{aligned}
 -1 \leq & \frac{K_1}{36} + \frac{\lambda\alpha_2 K_2(-1 + c_1 - 4c_2)}{24} \\
 & + \frac{\lambda^2\alpha_2^2}{12}[c_1 - 4c_2 + (\text{dex} - 1)(4c_2 - c_1^2 - 4c_1c_2)] \\
 & - \frac{\lambda^3\alpha_2^3}{72}[-1 + 3(1 - 2c_1)(c_1 + 4c_2)] \leq 1.
 \end{aligned} \tag{100}$$

for $\omega_i = \pm 1$, $i = 1, 2$, and in the cases $|\lambda\alpha_2| \gg 1$, $\lambda\alpha_2 \approx -1$ and $|\lambda\alpha_2| \ll 1$:

1. Upper bound, $\omega_1 = \omega_2 = 1$: $K_1 = 36$, $K_2 = 0$, $\text{dex} = 1$.
 For $|\lambda\alpha_2| \ll 1$, we require $c_1 - 4c_2 \leq 0$.
 For $|\lambda\alpha_2| \gg 1$, we require $-1 + 3(1 - 2c_1)(c_1 + 4c_2) \leq 0$.
 For $\lambda\alpha_2 \approx -1$, previous derived conditions in this appendix are sufficient.
2. Upper bound, $\omega_1 = \omega_2 = -1$: $K_1 = 4$, $K_2 = 8$, $\text{dex} = 1$.
 For $|\lambda\alpha_2| \ll 1$, we require $\lambda\alpha_2(-1 + c_1 - 4c_2) \leq 8/3$.
 For $|\lambda\alpha_2| \gg 1$, previous derived conditions are sufficient.
 For $\lambda\alpha_2 \approx -1$, we require $0 \leq 41 + 18(c_1 - 4c_2) - 3(1 - 2c_1)(c_1 + 4c_2)$. Taking into account previous derived conditions, it is sufficient to require $-20/9 \leq c_1 - 4c_2$.
3. Upper bound, $\omega_1 = 1 = -\omega_2$ or $\omega_2 = 1 = -\omega_1$: $K_1 = -12$, $K_2 = 8$, $\text{dex} = -1$.
 For $|\lambda\alpha_2| \ll 1$, previous derived conditions are sufficient.
 For $|\lambda\alpha_2| \gg 1$, previous derived conditions are sufficient.
 For $\lambda\alpha_2 \approx -1$, we require $0 \leq 73 + 18c_1^2 - 180c_2 + 9c_1(3 + 8c_2)$.
4. Lower bound, $\omega_1 = \omega_2 = 1$: $K_1 = 36$, $K_2 = 0$, $\text{dex} = 1$.
 For $|\lambda\alpha_2| \ll 1$, we require $-24 \leq \lambda^2\alpha_2^2(c_1 - 4c_2)$.
 For $|\lambda\alpha_2| \gg 1$, we require $\lambda^3\alpha_2^3[-1 + 3(1 - 2c_1)(c_1 + 4c_2)] \leq 144$. This condition will be satisfied by following ones.
 For $\lambda\alpha_2 \approx -1$, we require $0 \leq 9c_1 - 12c_2 - 6c_1^2 - 24c_1c_2 + 143$.
5. Lower bound, $\omega_1 = \omega_2 = -1$: $K_1 = 4$, $K_2 = 8$, $\text{dex} = 1$.
 For $|\lambda\alpha_2| \ll 1$, previous derived conditions are sufficient.
 For $|\lambda\alpha_2| \gg 1$, we require $\lambda^3\alpha_2^3[-1 + 3(1 - 2c_1)(c_1 + 4c_2)] \leq 80$. This condition will be satisfied by following ones.
 For $\lambda\alpha_2 \approx -1$, we require $0 \leq 103 - 15c_1 - 6c_1^2 + 84c_2 - 24c_1c_2$.
6. Lower bound, $\omega_1 = 1 = -\omega_2$ or $\omega_2 = 1 = -\omega_1$: $K_1 = -12$, $K_2 = 8$, $\text{dex} = -1$.
 For $|\lambda\alpha_2| \ll 1$, previous derived conditions are sufficient.
 For $|\lambda\alpha_2| \gg 1$, we require $\lambda^3\alpha_2^3[-1 + 3(1 - 2c_1)(c_1 + 4c_2)] \leq 48$.
 For $\lambda\alpha_2 \approx -1$, we require $0 \leq 6c_1^2 - 15c_1 + 36c_2 + 24c_1c_2 + 71$.

Acknowledgements This work was supported by the Collaborative Research Center on Gravitational Wave Astronomy of the Deutsche Forschungsgemeinschaft (DFG SFB/Transregio 7), the Spanish Ministerio de Educación y Ciencia (AYA 2010-21097-C03-01) the Generalitat Valenciana (PROMETEO-2009-103 and PROMETEO-2011-083) and the ERC Starting Grant CAMAP-259276. I. C.-C. acknowledges support from Alexander von Humboldt Foundation.

References

1. Butcher, J.C.: Numerical Methods for Ordinary Differential Equations, 2nd edn. J. Wiley, Chichester (2008)
2. Asher, U.M., Ruuth, S.J., Wetton, B.T.R.: Implicit-explicit methods for time-dependent PDE's. *SIAM J. Num. Anal.* 32, 797 (1995)
3. Asher, U.M., Ruuth, S.J., Spiteri, R.J.: Implicit-explicit Runge-Kutta methods for time-dependent partial differential equations. *Appl. Num. Math.* 25, 151 (1997)
4. Pareschi, L.: Central differencing based numerical schemes for hyperbolic conservation laws with relaxation terms. *SIAM J. Num. Anal.* 39, 1395 (2001)
5. Pareschi, L., Russo, G.: Implicit-explicit Runge-Kutta methods and application to hyperbolic systems with relaxation. *J. Sci. Comput.* 25, 129 (2005)
6. Gottlieb, S., Shu, C.-W.: Total Variation Diminishing Runge-Kutta schemes. *Math. Compt.* 67, 73–85 (1998)
7. Gottlieb, S., Shu, C.-W., Tadmor, E.: Strong-stability-preserving high order time discretization methods. *SIAM Review* 43, 89–112 (2001)
8. Shu, C.-W., Osher, S.: Efficient implementation of essentially non-oscillatory shock-capturing schemes. *J. Comput. Phys.* 77, 439 (1988)
9. Ruuth, S.J., Spiteri, R.J.: High-order strong-stability-preserving Runge-Kutta methods with downwind-biased spatial discretizations. *SIAM J. Numer. Anal.* 42, 974 (2004)
10. Kennedy, C.A., Carpenter, M.H.: Additive Runge-Kutta schemes for convection-diffusion-reaction equations. *Appl. Numer. Math.* 44, 139–181 (2003)
11. Hundsdorfer, W., Verwer, J.G.: Numerical Solution of Time-Dependent Advection-Diffusion-Reaction Equations. Springer-Verlag, Berlin (2003)
12. Handbook of Mathematical Functions with Formulas, Graphs, and Mathematical Tables. Abramowitz, M., Stegun, I.A. (eds.), pp. 878–879, and 883. Dover, New York (1972)
13. Kreiss, H.-O., Olinger, J.: Methods for the Approximate Solution of Time Dependent Problems. World Meteorological Organization, New York (1973)
14. Cordero-Carrión, I., Cerdá-Durán, P., Ibáñez, J.M.: Gravitational waves in dynamical spacetimes with matter content in the Fully Constrained Formulation. *Phys. Rev. D* 85, 044023 (2012)
15. Bonazzola, S.,ourgoulhon, E., Grandclément, P., Novak, J.: Constrained scheme for the Einstein equations based on the Dirac gauge and spherical coordinates. *Phys. Rev. D* 70, 104007 (2004)